Polymer Degradation and Stability 150 (2018) 92–104

Contents lists available at ScienceDirect

Polymer Degradation and Stability

journal homepage: www.elsevier.com/locate/polydegstab

Peculiar effect of stereocomplexes on the photochemical ageing of PLA/PMMA blends

Géraldine Rapp[a], Cédric Samuel[b], Jérémy Odent[c], Jean-Marie Raquez[c], Philippe Dubois[c], Pierre-Olivier Bussiere[a], Jean-Luc Gardette[a], Sandrine Therias[a,*]

[a] Université Clermont Auvergne, CNRS, SIGMA Clermont, ICCF, F-63000 Clermont-Ferrand, France
[b] Department of Polymers and Composites Technology and Mechanical Engineering (TPCIM), Mines Douai, Rue Charles Bourseul 941, CS 10838, 59508 Douai, France
[c] Laboratory of Polymeric and Composite Materials (LPCM), Center of Innovation and Research in Materials and Polymers (CIRMAP), University of Mons Research Institute for Materials Science and Engineering & Materia Nova Research Center (UMONS − MATERIANOVA), Place du Parc 23, B-7000 Mons, Belgium

ARTICLE INFO

Keywords:
Polylactide/poly(methyl methacrylate) blends
Stereocomplex
Morphology
Photodegradation

ABSTRACT

The effect of UV light on polylactide/poly(methyl methacrylate) (PLA/PMMA) blends produced by melt-extrusion with a special emphasis on the peculiar influence of PLA stereocomplexes on the photochemical behavior of the blends is the focus of this paper. Stereocomplexable PLA have been prepared by melt-blending of high-molecular-weight poly(L-lactide) (PLLA), poly(D-lactide) (PDLA) and PMMA. The photochemical behavior of resulting PLA/PMMA blends was studied by irradiation under photooxidative conditions ($\lambda > 300$ nm, temperature of 70 °C and in the presence of oxygen). The chemical modifications induced by UV light irradiation were analyzed using infrared spectroscopy (IR) and size exclusion chromatography (SEC). Morphological changes were studied by differential scanning calorimetry (DSC) and atomic force microscopy (AFM). It was shown that PDLA and PMMA don't affect the rate of photooxidation of PLLA. However, PLA stereocomplexes have a strong impact on the morphology of the blends during photochemical ageing.

1. Introduction

Driven by environmental awareness and fossil resources rarefaction, serious attention from industries has been paid to polylactide (PLA) as a biosourced alternative to conventional petroleum-based polymers in different types of applications such as packaging, automotive and electronics [1,2]. The reason for its development relies mainly on a number of interesting properties, including its excellent mechanical properties, positive life cycle assessment and relatively low-cost. Despite these advantages, some efforts on improving its thermal stability, impact strength, gas barrier properties or durability still need to be addressed. Among strategies to tune up the PLA performances in an efficient manner, PLA nanocomposites have been studied [3–10] and they represent a promising route to obtain new PLA grades with specific properties. However, polymer blending is probably the most extensively used methodology, especially in industries [11–13]. This prompted us to investigate polymer blends made of PLA and petro-based poly(methyl methacrylate) (PMMA) as an interesting approach to implement the resulting PLA-based materials into high-added value applications [14–18].

Recently, some of us have re-evaluated the miscibility extent between both PLA and PMMA upon either solvent-casting or twin-screw microcompounding [14]. While the solvent-casting method proved only able to produce immiscible blends, miscible PLA/PMMA blends were recovered all over the composition range once melt-processed [14]. As a result, homogeneous and transparent PLA/PMMA blends were produced with tunable thermo-mechanical performances and barrier properties. Some other efforts on using miscible PLA/PMMA blends as an alternative platform to design multiple shape-memory polymers (SMPs) were further addressed [19]. Broad glass transitions are classically encountered for miscible polymer blends [14,20–23]. Here, the symmetric 50/50 wt% PLA/PMMA formulations presented the broadest glass transition to finally demonstrated high triple-shape memory performances with tunable intermediate shapes. Going ever further, Hao et al. [16,17] investigated the effects of crystallinity and molecular entanglement on the shape memory performances of PLA/PMMA blends. While the molecular entanglement seems to have a positive influence on the shape memory performance, it is shown that the crystallization extent might hinder the shape recovery capability.

The latter pushed one of us to investigate the crystallization of PLA

* Corresponding author. I.C.C.F, UMR 6296, Institut de Chimie de Clermont-Ferrand, Université Clermont Auvergne, CNRS, SIGMA Clermont, Campus des Cézeaux, 24, avenue Blaise Pascal, TSA 60026, CS 60026, 63178 Aubière Cedex, France.
E-mail address: sandrine.therias@uca.fr (S. Therias).

https://doi.org/10.1016/j.polymdegradstab.2018.02.005
Received 11 December 2017; Received in revised form 22 January 2018; Accepted 7 February 2018
Available online 08 February 2018
0141-3910/

stereocomplexes upon the addition of PMMA [22]. The as-prepared ternary blends were found to be miscible, and such miscibility is likely a key factor to the role of PMMA in enhancing stereocomplexation. As such, stereocomplex crystallization into miscible PLLA/PDLA/PMMA blends represents a relevant approach to developing transparent, heat-resistant, and partly bio-based polymers using conventional technologies [24,25].

Since the PLLA/PDLA/PMMA ternary blends could fulfill, to some extent, requirements for industrial-scale injection-molding processes, it is important to have information about their stability over times. The resistance to ageing, especially UV light, is a key factor for outdoor applications of polymeric materials as degradation shortens the use-life of polymer-based products [26]. Thanks to the success of PLA in different fields (e.g. packaging, biomedical, engineering), numerous investigations have been devoted to the ageing of PLA-based materials under different conditions of degradation, e.g. hydrolytic, enzymatic, microbial, UV irradiation, photo-oxidative, natural weathering [27–35]. Photodegradation of PLA stereocomplexes have received less attention in terms of reaction mechanisms [36]. Concerning PMMA, a previous study has been reported in the literature [37], even though the mechanism of photooxidation is not completely solved yet.

The work reported in this article is the first investigation of the ageing of PLA/PMMA blends, especially once we consider PLA stereocomplex, under photooxidative conditions. The paper aims at studying the influence of stereocomplexes on the photooxidation of PLA/PMMA blends. The chemical modifications were followed by infrared (IR) analysis and Size Exclusion Chromatography (SEC) while Differential Scanning Calorimetry (DSC) and Atomic Force Microscopy (AFM) were performed to characterize the morphology of the blends upon photooxidation. A peculiar attention was paid to the influence of PDLA and PLLA in stereocomplex blends on the miscibility of the polymers in the blends.

2. Experimental section

2.1. Materials

A commercially available extrusion-grade poly(L-lactide) (NatureWorks 4032D), hereafter called PLLA, was used as received (Mn = 133500 ± 5000 g mol^{-1}, Đ = 1.94 ± 0.06 as determined by size-exclusion chromatography, 1.4 ± 0,2% D-isomer content as determined by the supplier). Poly(methyl methacrylate) (grade 8N, Mn = 52000 g mol^{-1} and Mw = 97000 g mol^{-1}), hereafter called PMMA, was supplied by Evonik. Ultranox 626A, supplied by GE Speciality Chemicals, was selected as the thermal stabilizer and used at ca. 0.3 wt% in all blends.

2.2. Synthesis of poly(D-lactide)

D,D-lactide was supplied by Purac (Purasorb D, purity 99.5%) and conserved in a glove box [14]. Bis(2-ethylhexanoate)tin(II) (stannous octanoate, Sn(Oct)2, Aldrich, purity 95%) and triphenylphosphine (Aldrich, purity 99%) were used for the synthesis of poly(D-lactide), hereafter called PDLA (D isomer > 99.9%, Mn = 35000 g mol^{-1} and Mw = 67000 g mol^{-1}). Polymerisation was carried out by reactive extrusion [38]. D-lactide was previously mixed with Ultranox 626 stabiliser and rapidly filled into previously flame dried and nitrogen purged glass bulbs, equipped with a stopcock capped with a rubber septum. The catalyst solution is added by a syringe with stainless steel capillary. Toluene was distilled off under reduced pressure for 60 min. The prepared mixture is transferred into a constantly nitrogen purged gravimetric feeding unit, which constantly provides the test-specific-throughput to the twin-screw extruder used as polymerisation device. The polymerisation occurs during the extrusion process at a temperature of about 185 °C. Finally, at the tip of the screw, the machine is equipped with a static mixer to homogenise the material and especially to improve distribution of the stabilising system in the PLA polymer. The polymer is extruded through a strand die, cooled by a constant flow of air on a take-off unit and pelletized.

Table 1
Materials, sample thickness, glass transition temperatures and melting temperatures.

	Thickness (μm)	T_g (°C)	T_m (°C)
100 PLLA	254	59	164
60/40	222	65	165
30/30/40	226	66	217–232
100 PMMA	274	114	–

2.3. Melt-blending

Prior to extrusion, PLLA, PDLA and PMMA pellets were dried overnight at 60 °C under vacuum, and Ultranox 626A was dried overnight at 25 °C to minimize the water content in each component and avoid any excessive degradation upon further processing. Different formulations were targeted: pure PLLA (as denoted 100 PLLA), PLLA/PMMA 60/40 wt/wt% (as denoted 60/40 blend), PLLA/PDLA/PMMA 30/30/40 wt/wt/wt% (as denoted 30/30/40 blend) and pure PMMA (as denoted 100 PMMA). Respective blends were melt-processed at 210 °C (230 °C in presence of PDLA) and 60 rpm for 10 min under nitrogen flow using a twin-screw micro-compounder (Xplore, 15 cc.) [22]. Circular samples (diameter 25 mm, thickness 200–250 μm) were produced by compression-molding at 190 °C for 100 PLLA, 210 °C for 60/40 and 230 °C for 30/30/40 and 100 PMMA (Table 1). At the exception of the 100 PMMA, all formulations were then annealed using the following procedure in order to reach the maximum crystallinity value for each sample: 1 h at 110 °C for 100 PLLA, 2 h at 110 °C for 60/40 and 30 min at 110 °C for 30/30/40.

2.4. Photochemical ageing

Films were irradiated at λ > 300 nm in presence of oxygen in a SEPAP 50-24 unit from Atlas [39]. This device is equipped with eight medium pressure mercury lamps located around the rotating carrousel which holds the samples. A borosilicate envelope filters the UV-light with wavelengths below 300 nm. The temperature at the surface of the samples was fixed at 70 °C (this temperature is below the T_g of PMMA (T_g = 115 °C) but above the T_g of PLA (T_g = 60 °C)). This device is specifically designed to study the photodegradation of polymers in artificial conditions corresponding to an ultra-accelerated ageing. As a reference, an acceleration factor of 50 was calculated for polyethylene films compared to natural ageing [40].

2.5. Characterisations techniques

IR analysis. Infrared spectra were recorded in transmission mode with a Nicolet 6700 FTIR spectrometer, working with OMNIC software, on films with thicknesses of around 200–250 μm. Spectra were obtained using 32 scans and a 4 cm^{-1} resolution.

Chemical treatments. The photooxidised samples were submitted to various chemical treatments in order to identify the photo-products. The irradiated 100 PMMA films (500 h in a SEPAP 50-24 device) were exposed to reactive gases such as ammonia (NH_3) and sulfur tetrafluoride (SF_4) at room temperature in a simple flow system that could be sealed off to permit the reaction to proceed. SF_4 and NH_3 treatments were carried out in an all-Teflon system. As a reference, non-irradiated 100 PMMA films were submitted to the same treatment to check that no reaction occurred with the reactive gases. As illustrated hereafter, the reaction of NH_3 with any carboxylic acid, ester or anhydride end-groups leads to the formation of ammonium carboxylates and/or amide groups, respectively.

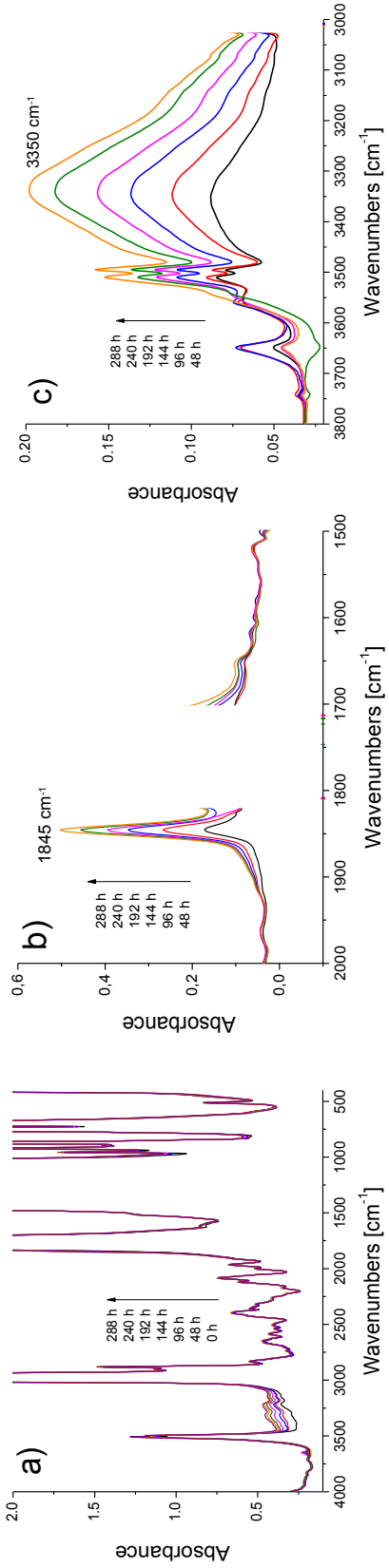

Fig. 1. IR spectra of PLLA films (e = 254 μm) during photooxidation at λ > 300 nm and 70 °C. a) direct spectra in the domain 4000–400 cm^{-1}. b) subtracted spectra (A_t-A_0) in the domain 2000–1500 cm-1 c) subtracted spectra (A_t-A_0) in the domain 3800–3000 cm^{-1}.

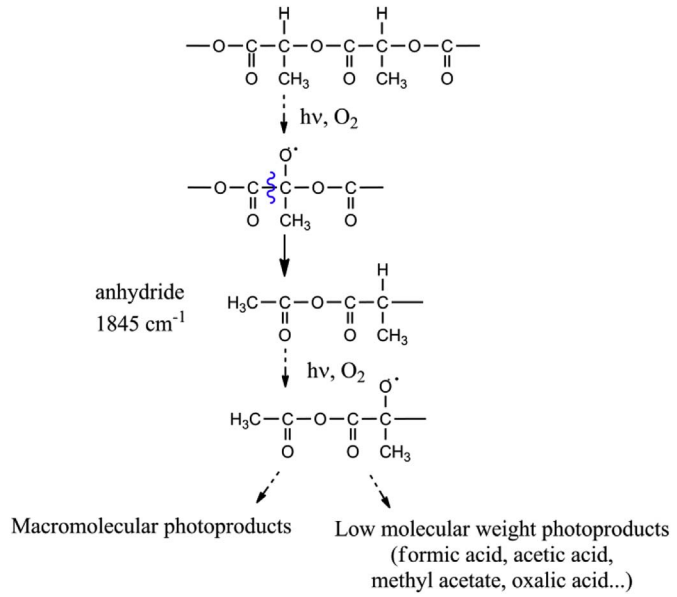

Scheme 1. Photoproducts of PLA from the comprehensive photooxidation mechanism of PLA [42].

$$RCOOH + NH_3RCOO^-,NH_4^+$$

$$RCOOR' + NH_3RCONH_2 + R'OH$$

$$RCO\text{-}O\text{-}CO\text{-}R' + 2NH_3RCOO^-,NH_4^+ + R'CONH_2$$

The resulting ammonium carboxylates are then characterized by an infrared absorption band between 1545 and 1560 cm^{-1} while the amide groups present among others, two characteristic absorption bands at 1670 and 1630 cm^{-1}. Besides, the reaction of carboxylic acid with SF_4 leads to the formation of acid fluorides. This treatment allows differentiating aliphatic acids from unsaturated acids. Aliphatic acid fluorides are characterized by an infrared absorption band around 1845 cm^{-1}, whereas unsaturated acid fluorides have an infrared absorption band around 1815 cm^{-1}.

$$RCOOH + SF_4RCOF + HF + SOF_2$$

Differential scanning calorimetry (DSC). The thermal characteristics of the films were determined by DSC from the first scan using a Mettler Toledo DSC 822e at a heating rate of 10 °C/min from 25 to 210 °C (240 °C in presence of PDLA). The events of interest, i.e. the glass transition temperature (T_g), melting temperature (T_m) and melting enthalpy (ΔH_m) were determined from the first scan in order to not cancel the effect of ageing on the morphology of the samples. Samples crystallinity was calculated from the heat of fusion using the following equation (1):

$$x(\%) = \frac{\Delta Hm}{\Delta Hm_{100\%}} \times 100 \quad (1)$$

where χ is the weight fraction crystallinity, ΔH_m is the melting enthalpy for the sample and $\Delta Hm_{100\%}$ is the melting enthalpy for a 100% crystalline PLA equal to 93.6 J g^{-1} [41].

In the case of stereocomplex 30/30/40 blend, $\Delta Hm_{100\%}$ of homo- and stereocomplex crystallites in the films have different values. The crystallinities ascribed to homo- and stereocomplex crystallites in the 30/30/40 blend were evaluated using 135 and 146 J g^{-1} respectively according to Tsuji et al. [42].

Size exclusion chromatography (SEC). The changes in the molecular weight for 100 PLLA, 100 PMMA and 30/30/40 blend were obtained by SEC using a Viscotek SEC-TDA chromatograph. It consists of a TDA 302 module (triple detector array) that includes a column oven (35 °C) and triple detector consisting of an RI detector (Viscotek VE 3580), a four-

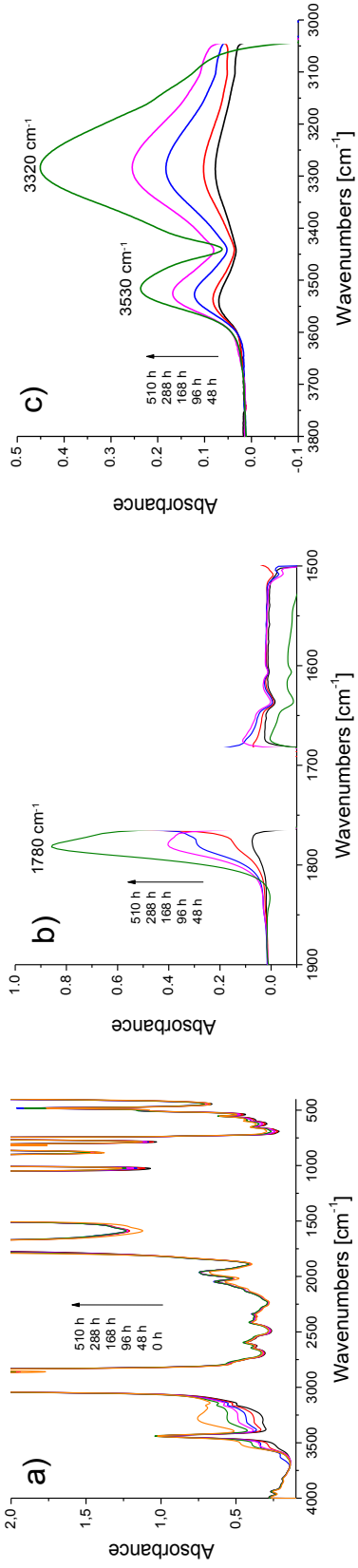

Fig. 2. IR spectra of PMMA films (e = 274 μm) during photooxidation at λ > 300 nm and 70 °C. a) direct spectra in the domain 4000–400 cm^{-1}. b) subtracted spectra (A_t-A_0) in the domain 2000–1500 cm-1 c) subtracted spectra (A_t-A_0) in the domain 3800–3000 cm^{-1}.

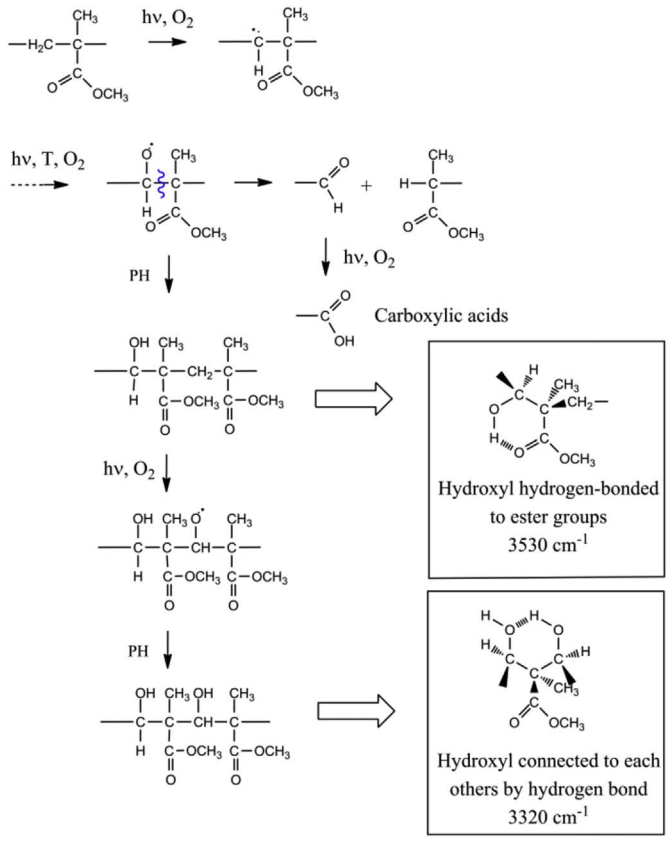

Scheme 2. Photooxidation products of PMMA [37].

bridge viscometer and LS detector (Viscotek TriSec Model 270 dual detector with a laser). The latter consisted of a right-angle light scattering (RALS) detector and an innovative low-angle light scattering (LALS) detector. Two TSK-GEL columns (GMHXL and G3000HXL) in series that were preceded by a TSK-GEL guard column HXL-L were used. The analyses were performed using THF as an eluent at a flow rate of 1 mL/min. The solutions were prepared in THF (10 mg polymer/5 mL solvent) and were filtered before injection. The OmniSEC software program was used for acquisition and analysis of the Viscotek data.

Atomic Force Microscopy (AFM). AFM measurements were done using a tapping mode Innova® Atomic Force Microscope (RTESPA-CP) from Bruker and a Bruker Multimode driven by Nanoscope V control unit. For Innova® Atomic Force Microscope analysis, typical technical data include (for the cantilever): thickness: 3.75 μm: length: 125 μm: width: 35 μm: resonance frequency: 300 kHz: force constant: 40 N/m. Each experiment was performed several times to ensure reproducibility. The surface topographical images of the films were worked up with Nanoscope Analysis 1.8 image processing software. RMS roughness (R_q) values for the surfaces, defined as the standard deviation of the z-piezo position value within a given area, were calculated according to equation (2):

$$R_q = \sqrt{\frac{\sum (Z_t - Z_{ave})^2}{N}} \quad (2)$$

where z_{ave} is the average of the z value within the given area, z_t is the z value for a given point, and N is the number of points within the given area. Four locations within each image were used to calculate the average roughness. For Bruker Multimode driven by Nanoscope V control unit, film surfaces were imaged in peak-force tapping mode which is based on real time force distance curve analysis. In this mode, the probe is oscillating near 300 kHz, capturing a force-distance curve while scanning the sample oscillating at low frequency (2 kHz). This allows us to locally measure various mechanical properties at nanoscale

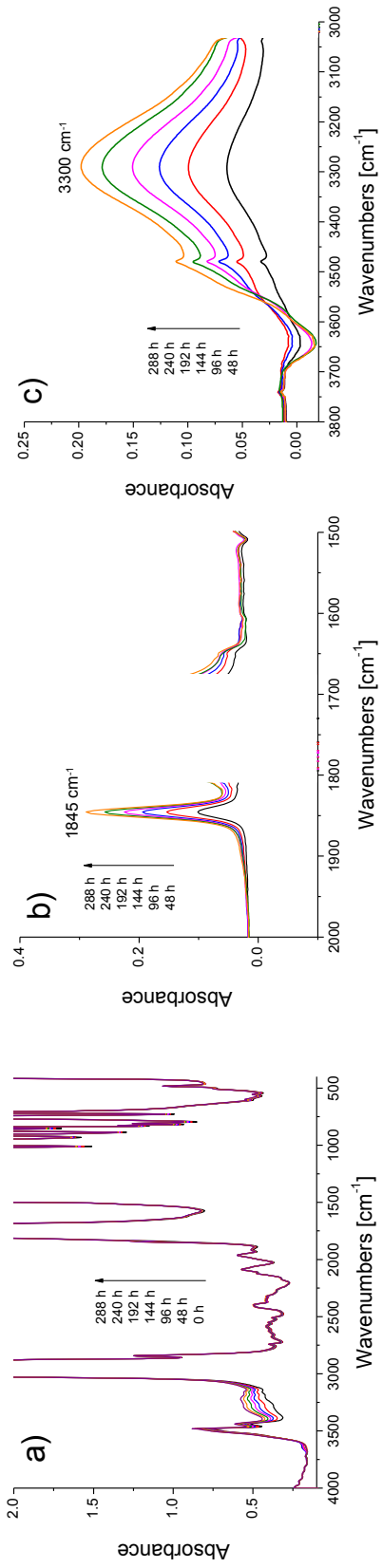

Fig. 3. IR spectra of 30/30/40 blend films (e = 226 μm) during photooxidation at λ > 300 nm and 70 °C. a) direct spectra in the domain 4000–400 cm^{-1}. b) subtracted spectra (A_t-A_0) in the domain 2000–1500 cm-1 c) subtracted spectra (A_t-A_0) in the domain 3800–3000 cm^{-1}.

such as Young's modulus (from data analysis based on DMT model), adhesion, deformation and dissipation, simultaneously to the height image. This technology also provides equal or higher resolution than a Tapping mode image. Topographic height images were recorded simultaneously to the modulus map of 512 × 512 pixels. The measurements were done in air and ambient conditions of pressure and temperature. The tip used was a RTESPA-300 cantilever (Bruker) with spring constant of approximately 40 N/m and a radius of curvature of approximately 8 nm.

3. Results and discussion

3.1. Chemical characterization of photoproducts of PLA/PMMA blends

3.1.1. Infrared analysis

Photooxidation products of 100 PLLA and 100 PMMA films were firstly characterized. Fig. 1a shows the IR spectra of 100 PLLA films during photooxidation. The modifications of the IR spectra in the carbonyl domain can be observed in subtracted spectra.

Fig. 1b (the spectrum of 100 PLLA before irradiation being subtracted) clearly revealed the formation of an IR absorption band at 1845 cm^{-1}. Photooxidation of PLA has already been studied [27,34,43], and this IR absorption band was assigned to anhydride functions. The second major modification of the spectra is observed in the hydroxyl region (Fig. 1c) showing a wide absorption band with a maximum at 3350 cm^{-1}, assigned to hydroxyl functions (alcohols, carboxylic acids).

A comprehensive mechanism of PLA photooxidation has already been proposed [43] taking into account the low molecular weight products that were also formed (Scheme 1). The analyses of the gas phase allowed for identifying the main volatile low molecular weight photoproducts such as carboxylic acids and methyl acetate [43].

Fig. 2 shows the IR spectra of 100 PMMA films during photooxidation. The formation of IR absorption bands were observed in the hydroxyl domain at 3520 cm^{-1} and 3280 cm^{-1}.

The PMMA photodegradation has been studied by Siampiringue et al. [37] who reported the formation of a narrow band at 3530 cm^{-1} and a wide band centered at 3320 cm^{-1}. These IR bands were ascribed to hydroxyl groups of hydroperoxides or alcohol or carboxylic acid functions that are connected by an hydrogen bond to ester groups (3530 cm^{-1}) or connected to each other's (3320 cm^{-1}) (Scheme 2).

In the carbonyl domain (Fig. 2b), a new absorption band develops at 1780 cm^{-1} which can be attributed to lactones formation.

Blends of 60/40 PLLA/PMMA (as named 60/40) and 30/30/40 PLLA/PDLA/PMMA (as named 30/30/40), which display a stereocomplex morphology, were then characterized by IR analysis.

The same trends were observed for both blends. Fig. 3a illustrates the modifications of the IR spectrum during photooxidation of 30/30/40 PLLA/PDLA/PMMA blends. Fig. 3b shows the formation of an IR absorption band at 1845 cm^{-1} and Fig. 3c shows the formation of a broad band centered at 3300 cm^{-1}. The IR band at 1845 cm^{-1} corresponds to anhydride functions of PLA photooxidation products, as reported above, and is specific to PLA photooxidation. In the hydroxyl region (Fig. 3c), the IR band corresponds to photoproducts of both polymers in the blend (PLA and PMMA). The PMMA photoproducts at 1780 cm^{-1} cannot be observed due to the initial IR band at 1730 cm^{-1}, corresponding to the ester functions of both PLA and PMMA.

3.1.2. IR analysis after chemical treatments

Chemical treatments were carried out on the photooxidised films (chemical derivatization) to identify and confirm the chemical functions of the photoproducts. Chemical treatment with NH_3 gas on PLA photooxidised films has already been reported by Gardette et al. [27] and confirmed the presence of anhydride functions formed during PLA photooxidation. Fig. 4 presents the IR spectra of a 500 h photooxidised 100 PMMA film before and after chemical treatment with NH_3 and SF_4

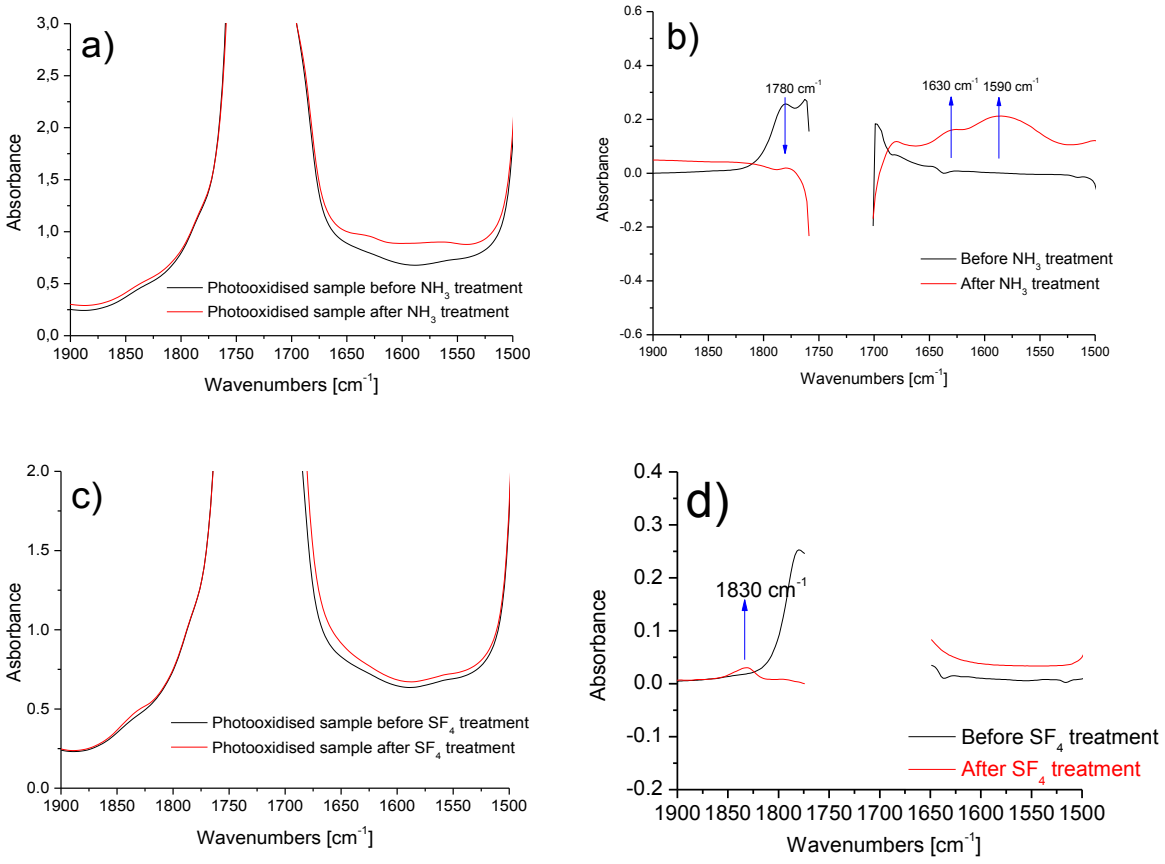

Fig. 4. FTIR spectra of photooxidised 100 PMMA films (500 h) before and after treatment with NH_3 (a and b) and SF_4 (c and d). a) and c) direct spectra in the domain 1900–1500 cm^{-1}. b) and d) subtracted spectra (A_t-A_0) in the domain 1900–1500 cm^{-1}.

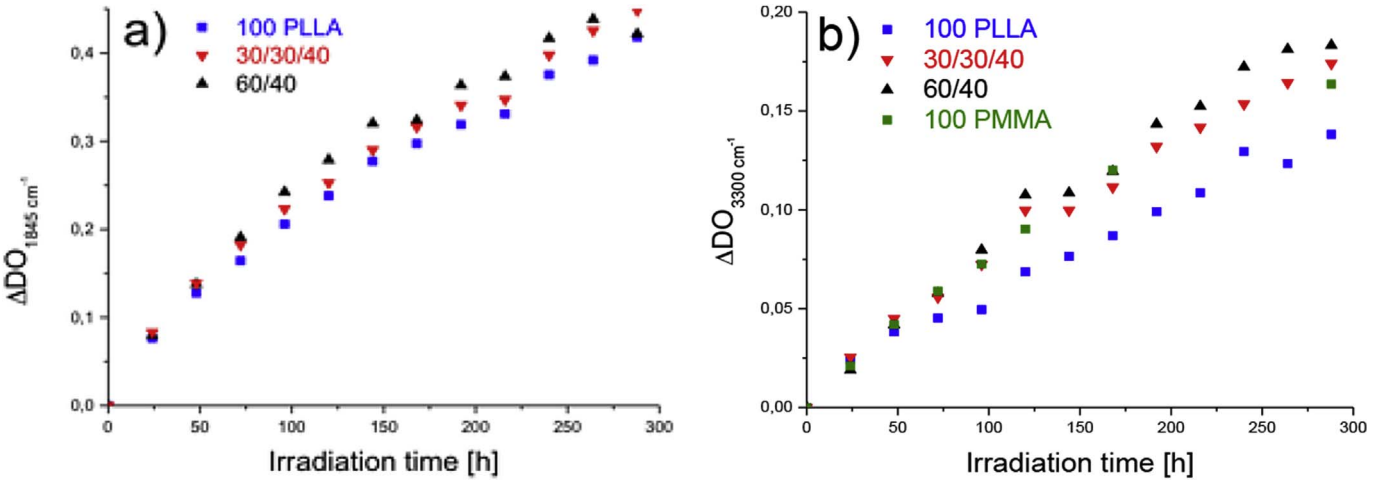

Fig. 5. Variations of absorbance as a function of irradiation time a) at 1845 cm^{-1} for 100 PLLA, 60/40 and 30/30/40, with correction of thickness and PLA amount. b) at 3300 cm^{-1} for 100 PLLA, 30/30/40, 60/40 and 100 PMMA, only with correction of thickness.

gas.

After NH_3 treatment of PMMA films (Fig. 4a and b), one can observe an increase of absorbance between 1675 and 1500 cm^{-1} in the IR spectra. Regarding the subtracted spectra (Fig. 4b), we can notice a decrease of the band at 1780 cm^{-1} and the appearance of two new absorption bands at 1630 cm^{-1} and 1590 cm^{-1}. These IR bands correspond to amide and carboxylate functions respectively. These modifications indicate the reaction of carboxylic acids and esters or anhydrides functions with NH_3. After SF_4 treatment of PMMA films (Fig. 4c and d), we observe in the IR spectrum the formation of a new absorption band at 1830 cm^{-1}. These modifications indicated the presence of aliphatic carboxylic acids as photoproducts in PMMA.

3.2. Kinetics of photooxidation of PLA/PMMA blends

The kinetic curves of oxidation were plotted at 1845 cm^{-1} (Fig. 5a) and 3300 cm^{-1} (Fig. 5b). In Fig. 5a, the variations of absorbance at 1845 cm^{-1} have been plotted for 100 PLLA, 60/40 and 30/30/40

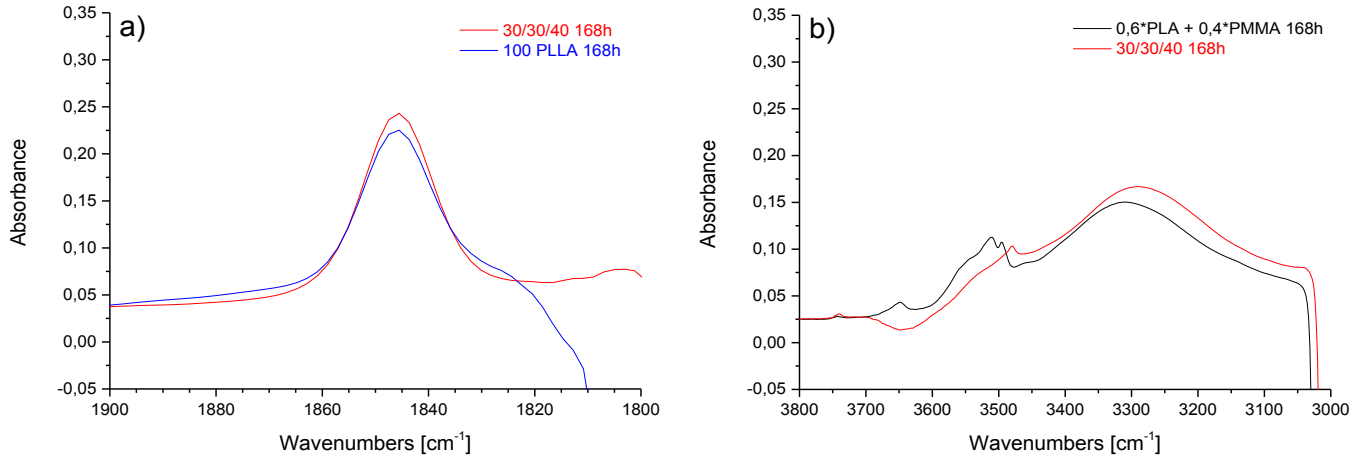

Fig. 6. a) FTIR spectra of photooxidised 100 PLLA and 30/30/40 films (168 h) in the domain 1900–1800 cm^{-1}. b) FTIR spectrum of photooxidised 30/30/40 film (168 h) compared to calculated spectrum 0.6*PLA + 0.4*PMMA (after 168 h of irradiation).

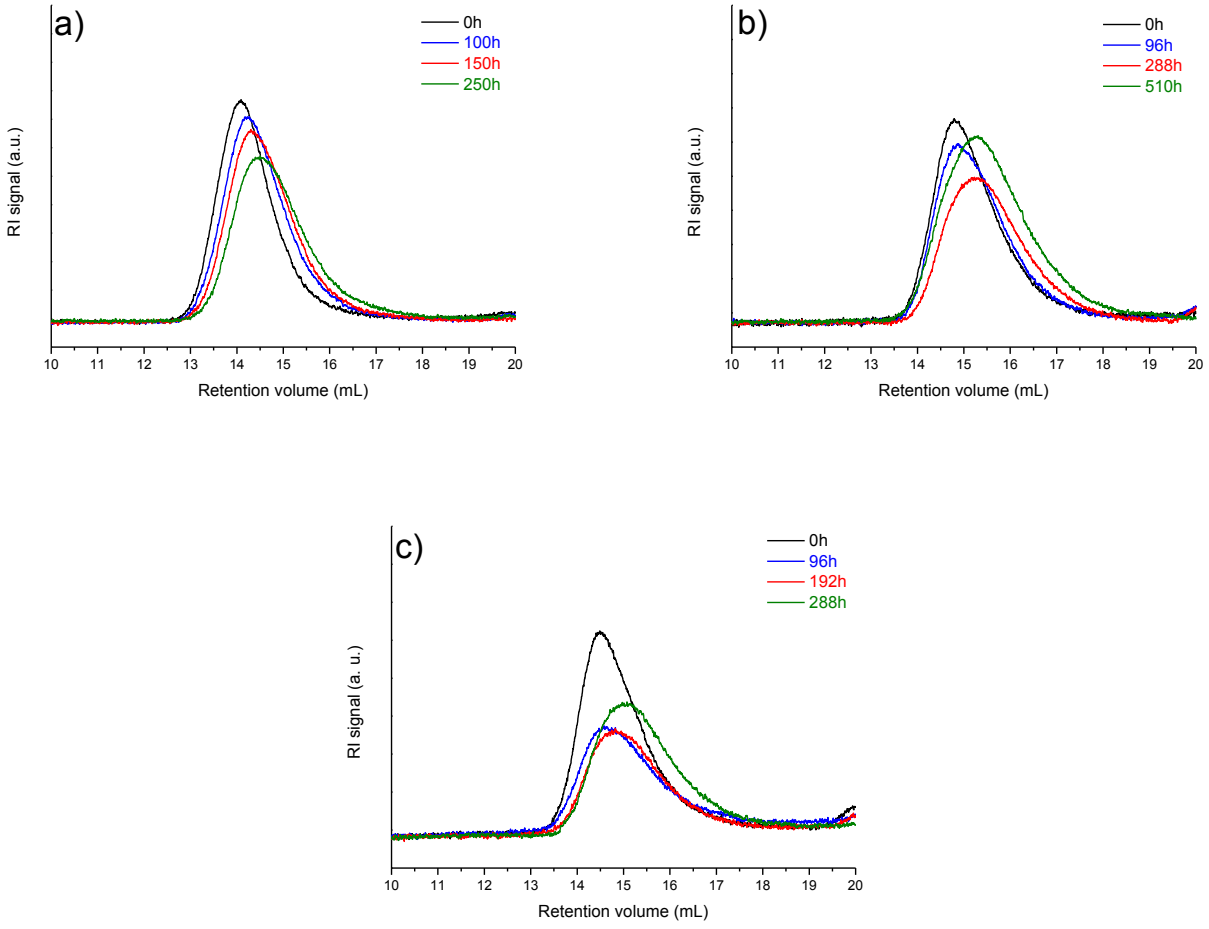

Fig. 7. Variations of RI signal during photoageing for a) 100 PLLA and b) 100 PMMA c) 30/30/40 blend.

blends. This IR band reflects the photooxidation of PLA. The values have been multiplied by two correction factors, successively applied in order to compare films with a same thickness (e = 220 µm), and with the same amount of PLLA. One can observe that the variations of absorbance are the same for the pristine PLLA and the blends. This means that neither PDLA nor PMMA affect the rate of photooxidation of PLLA.

In Fig. 5b, the variations of absorbance at 3300 cm^{-1} are plotted for 100 PLLA, 60/40, 30/30/40 blends and 100 PMMA. This IR band corresponds to hydroxyl oxidation products formed during both PLA and PMMA photooxidation. The curves were only corrected once in order to compare films with a same thickness (e = 220 µm). This allows us to compare the contribution of both polymers to the degradation of

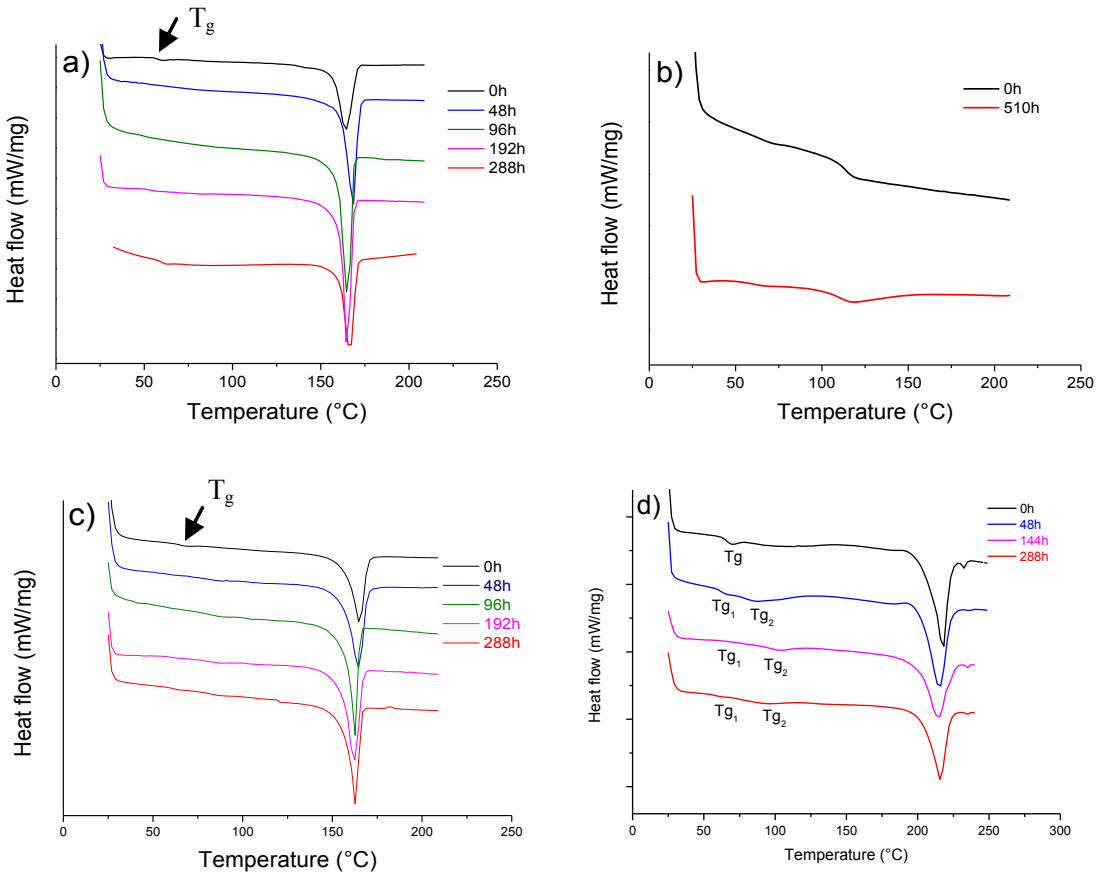

Fig. 8. DSC thermograms of a) 100 PLLA b) 100 PMMA c) 60/40 d) 30/30/40 during photooxidation.

Table 2
Molecular weight and crystallinity degree of PLLA/PDLA/PMMA annealed blends. DSC analyses of the films during photooxidation are presented in Fig. 8, and the main thermal parameters are gathered in Table 3.

	Molecular weight Mw ($g.mol^{-1}$)	Crystallinity degree (%)
100 PLLA	218000	47
60/40	–	56
30/30/40	–	63
100 PMMA	97000	–

Table 3
Selected DSC data obtained by characterization of 100 PLLA, 100 PMMA, 60/40 and 30/30/40 films with different ageing histories (first heating with a ramp of 10 °C/min).

	T_g (°C)	T_m (°C)	ΔH_m ($J.g^{-1}$)	χ (%)
PLLA				
0 h	59	164	44	47
48 h	–	168	54	57
96 h	50	165	67	71
192 h	54	165	64	68
288 h	60	166	50	53
PMMA				
0 h	114	–	–	–
510 h	111	–	–	–
60/40				
0 h	65	165	53	56
48 h	–	164	69	74
96 h	–	162	63	68
192 h	62	162	71	76
288 h	62	163	62	66
30/30/40				
0 h	66	217–233	82 + 2	63
48 h	62–79	215–236	82 + 1	61
144 h	76–97	215–235	69 + 1	51
288 h	58–86	216–235	63 + 1	47

the blend. Fig. 5b shows that at 3300 cm^{-1}, PLLA gives rise to less hydroxylated photoproducts than PMMA. The rates of oxidation of the 60/40, 30/30/40 blends and 100 PMMA are very similar, whereas that of PLLA is slightly lower. In PLA/PMMA blends, more hydroxylated photoproducts are formed, however the presence of PDLA has no specific effect and there is no prodegradant effect in the case of the stereocomplex blend. It is important to note that PLA and PMMA have similar kinetics of photooxidation and long ageing times are required to see photooxidation products in both polymers. PLA and PMMA are both photostable. One question that comes into play is to known if PLA and PMMA have a reciprocal influence that could provoke an increased oxidation of both the components. For that, we have compared the absorbance at 1845 cm^{-1} (attributed to PLA) in 100 PLLA and 30/30/40 blend after 168 h of irradiation, the values being corrected to have the same amount of PLA (Fig. 6a). The conclusion was that the rate of photooxidation of PLA was not modified in the blend. This allowed us to calculate the participation of the products issued from PLA to the absorbance in the hydroxyl domain at 3340 cm-1 in the blend, and then to extract the participation of the products from PMMA to this absorbance. The absorbance in the hydroxyl domain in the photooxidised blend was then compared to the calculated absorbance 0,6*PLA + 0,4*PMMA (Fig. 6b). The obtained result gave a similar value, which indicated that PLA had no influence on the oxidation rate of PMMA in the blends.

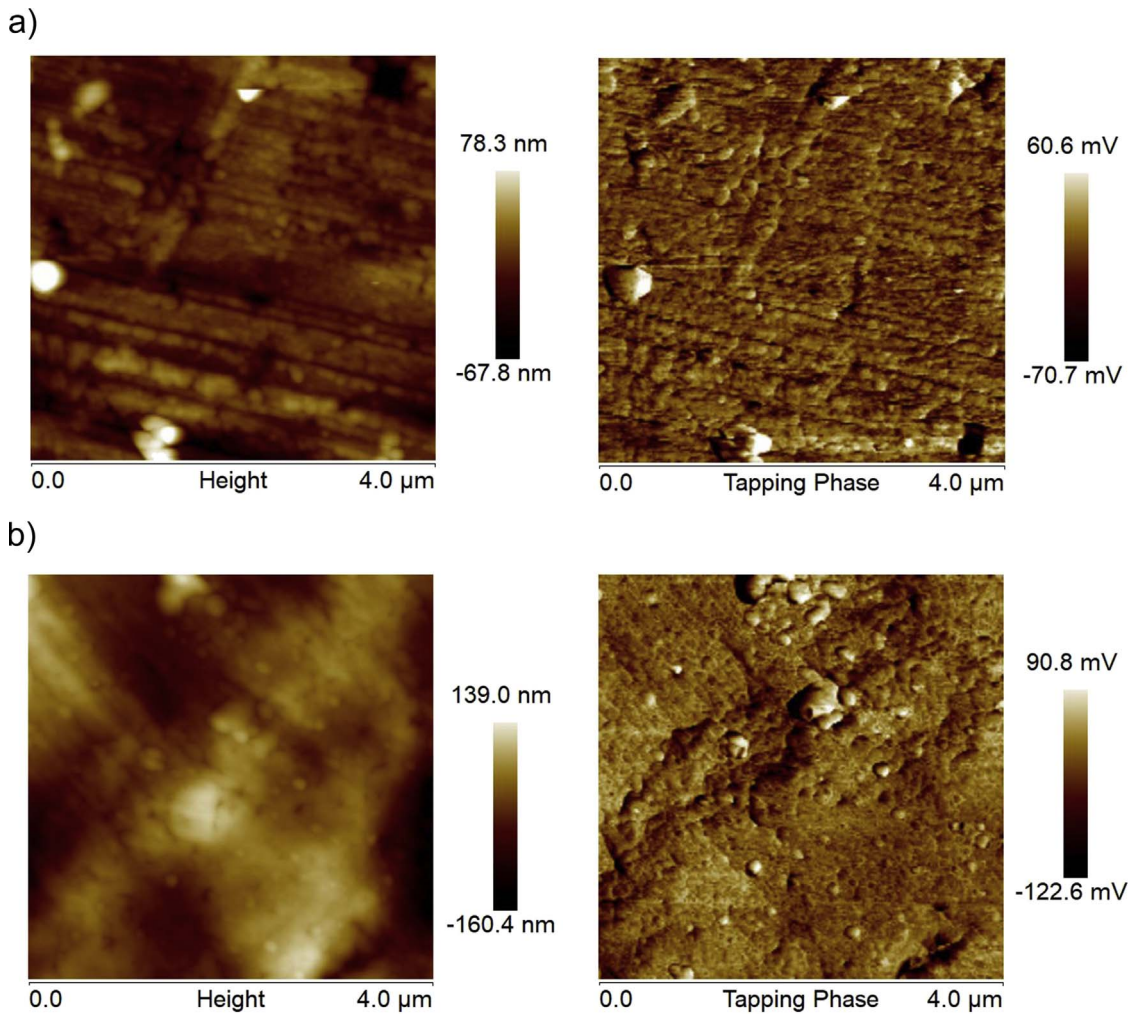

Fig. 9. AFM images (4 µm × 4 µm) of 60/40 blend a) before ageing and b) after 192 h of ageing.

3.3. Macromolecular architecture: molecular weight

Fig. 7 shows the chromatograms from the RI detector of 100 PLLA, 100 PMMA and 30/30/40 blend during photooxidation.

For 100 PLLA (Fig. 7a), one can observe that the elution peak progressively shifts towards higher retention volumes after photooxidation, which indicates a decrease of molecular weight. As previously reported [27,34], this decrease indicates that photooxidation of PLLA provokes chain scissions that are responsible for the formation of low molecular weight products.

100 PMMA film presents similar trends in the chromatograms (Figs. 7b) and 30/30/40 blend (Fig. 7c). One can conclude that, as for 100 PLLA, photooxidation of 100 PMMA and 30/30/40 blend leads to chain scissions.

3.4. Morphology of the blends after photooxidation

3.4.1. DSC analysis

Polymers and blends were annealed in order to increase their crystallinity and reach a stable value before ageing, which was confirmed by DSC measurements. Crystallinity increased from 3% to 47% for 100 PLLA, from 10% to 56% for 60/40 blend and from 0% to 63% for 30/30/40 blend. The main characteristics of the polymers are described in Table 2.

For 100 PLLA film (Fig. 8a), a decrease of the T_g value during phootooxidation can be observed (Table 3), due to the formation of low molecular weight products by degradation, as already observed by Gardette et al. [27]. Then, an increase of T_g is observed with a decrease of the crystallinity degree from 96 to 288 h of photooxidation. The T_m remained almost unchanged during irradiation. 100 PMMA films are amorphous and were characterized by a T_g on the DSC thermogram (Fig. 8b).

We can notice a slight decrease of the T_g after 500 h of ageing, which could reflect chain scissions during photooxidation of PMMA.

The 60/40 blend (Fig. 8c) shows a single glass transition before and after ageing, with a T_g that decreases upon ageing time, as observed for 100 PLLA. The T_g is almost invisible because of the high crystallinity of the sample and the slow heating rate (10 °C/min). Concerning melting temperature T_m and crystallinity degree, 60/40 blend behaves as 100 PLLA. T_m remains unchanged during irradiation while crystallinity increases after 288 h of ageing.

The unaged 30/30/40 ternary blend (Fig. 8d) shows a single glass transition at intermediate value between that of pure PLLA (60 °C) and pure PMMA (114 °C), which in accordance with Samuel et al. [22] and is characteristic of a miscible blend. One can observe two different glass transition temperatures after 48 first hours of ageing. After 288 h of ageing, the two T_g are even more separated and get closer to the T_g of pure PLLA and pure PMMA. In the case of ternary blend 30/30/40 PLLA/PDLA/PMMA, the presence of PLA stereocomplexes may lead to a phase separation during photochemical ageing, which has not been observed in the case of 60/40 PLLA/PMMA blend. Concerning the two melting temperatures, already observed for the unaged sample, they are not affected by the photochemical ageing. This means that the stereocomplex crystallites remain. The first peak, at around 216 °C,

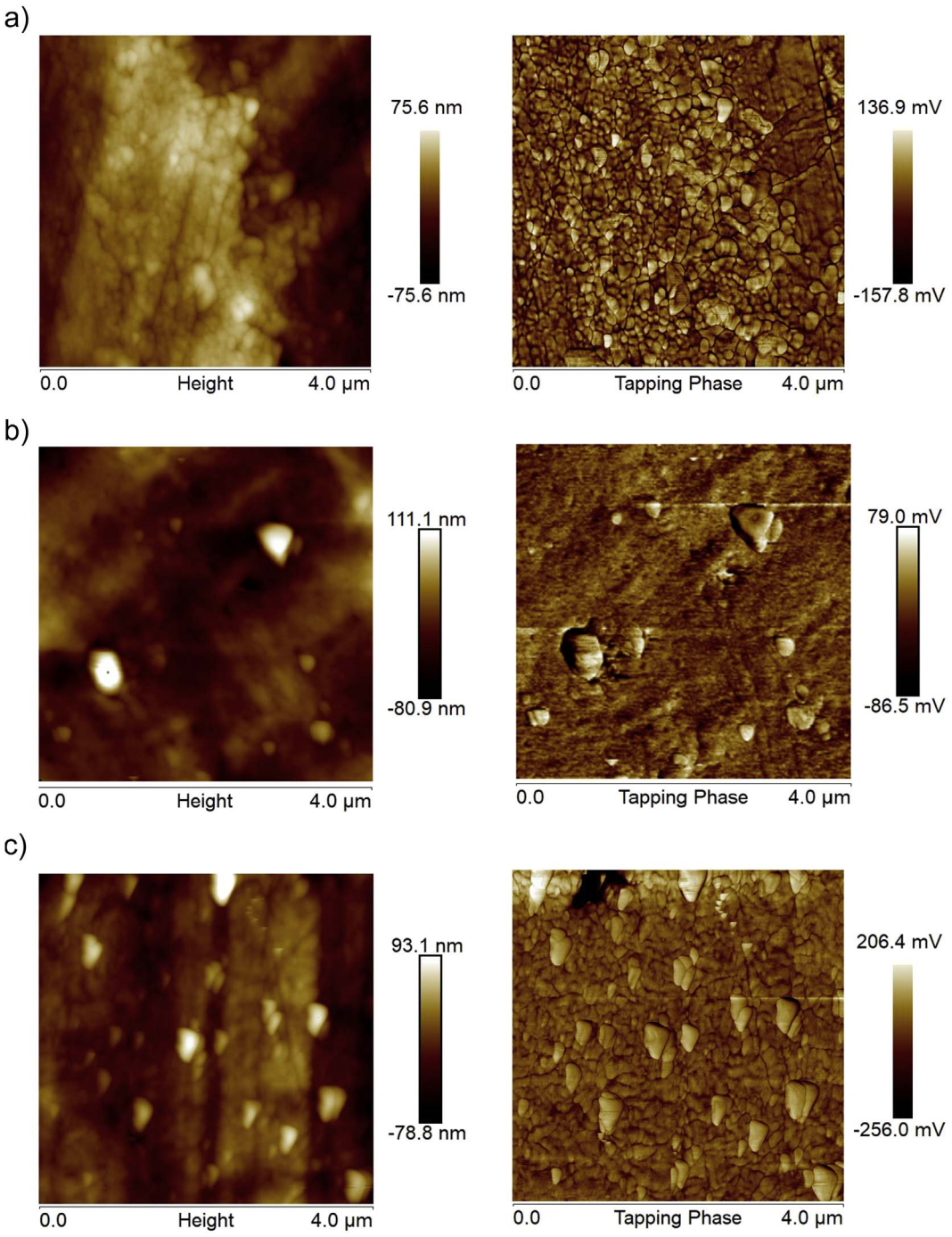

Fig. 10. AFM images (4 µm × 4 µm) of 30/30/40 blend a) before ageing b) after 192 h of ageing and c) after 288 h of ageing.

corresponds to crystals of PLA stereocomplexes, and the second one around 235 °C [22], which is smaller, to PLA homocrystallites. Whereas photoageing has no influence on the melting temperatures of the blend, the crystallinity degree of ternary 30/30/40 blend does not follow the same trend as 100 PLLA and 60/40 blend. Crystallinity decreases from 63% to 47% after 288 h of photochemical ageing. This result can directly be linked with the phase separation phenomenon, as the crystallinity in the blends only comes from PLA. This indicates that the presence of PLA stereocomplexes has a strong influence on the morphology of PLA/PMMA blends during photooxidation.

In order to check if the appearance of two T_g during ageing was due to a photooxidative or a thermooxidative process, a 30/30/40 blend film was submitted to thermal oxidation at 70 °C (temperature of the samples during irradiation in the photoageing device), and then analyzed in DSC. The thermogram presents only one T_g that is intermediate between that of pure PLLA and pure PMMA, as observed before ageing. Therefore, we can assume that the presence of two T_g after irradiation is due to a photochemical process, which may lead to a phase demixing phenomenon.

3.4.2. Atomic force microscopy images

Fig. 9 shows AFM height and phase images of 60/40 films before and after 192 h of irradiation.

The surface roughness of 60/40 blend increases from 33.5 ± 2.0 before ageing to 40.1 ± 3.0 after 192 h of photo oxidation, which can be related to a loss of low molecular weight products produced during

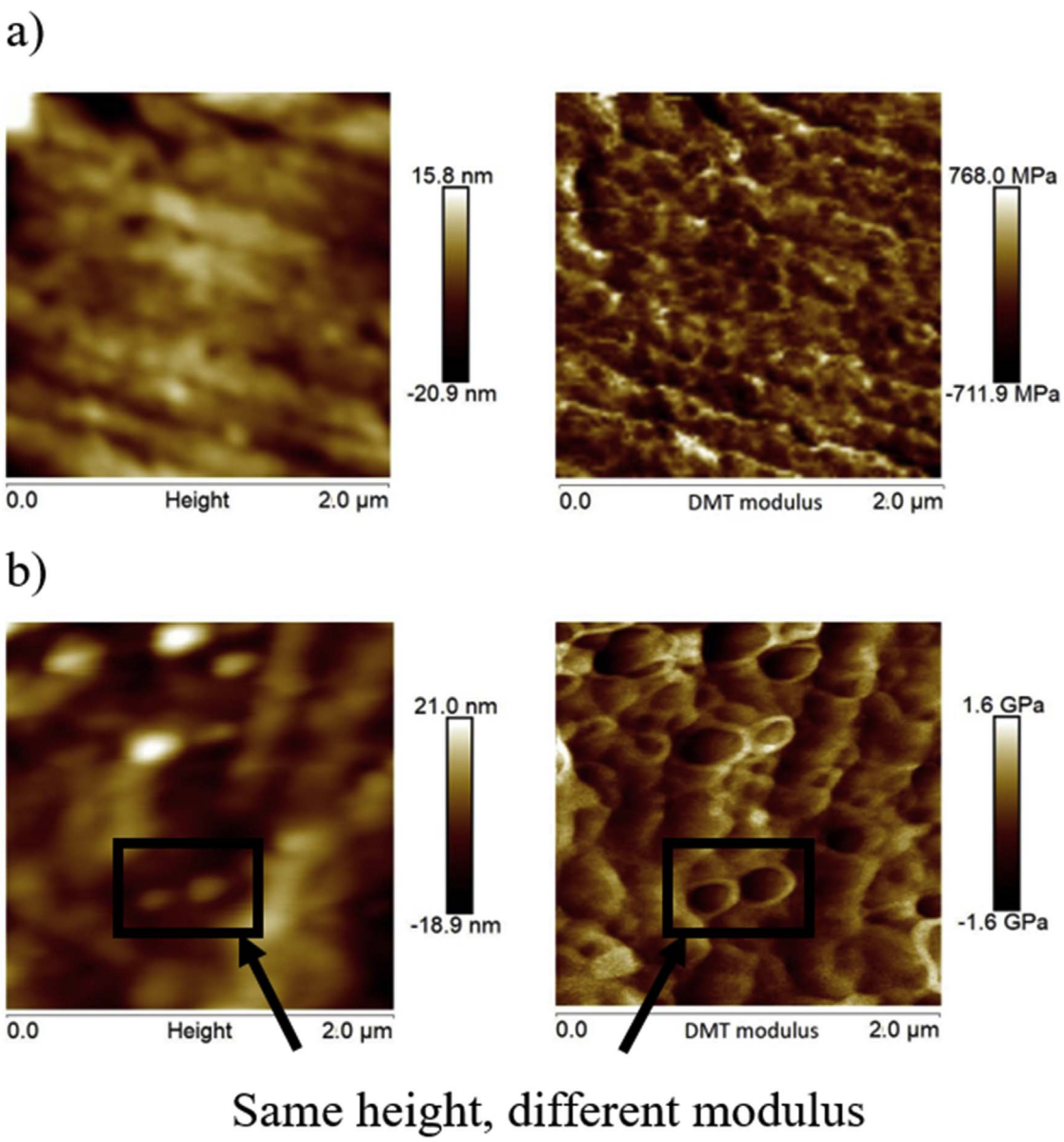

Fig. 11. AFM height and DMT modulus of a) 60/40 blend after 192 h of ageing and b) 30/30/40 blend after 192 h of ageing.

photooxidation. The migration of low molecular weight products and its consequences on the surface roughness have already been reported in the case of PVA photooxidation [44]. It can be anticipated that the loss of matter provokes internal stresses that release by creating microcracks at the surface, which induces an increase of the roughness. The AFM images of 60/40 blend after photoageing (Fig. 9b) show that no phase separation is observed. The blend remains homogeneous, which is consistent with the DSC analysis.

Fig. 10 shows AFM height and phase images of 30/30/40 blend films before and after 192 and 288 h of irradiation.

AFM images (Fig. 10a) indicate that the blend is highly crystalline. Due to the annealing process of the sample and the presence of stereocomplex crystallites with a melting temperature at 219 °C, this is consistent with the DSC results given above. Photooxidation has a strong influence on the surface roughness of the 30/30/40 films, which is even more important than that observed in the case of the 60/40 blend. The surface of the samples before UV-light irradiation is homogeneous and has a low roughness value (11.5 ± 3.0), with no obvious surface irregularities, whereas after 192 h of irradiation, the roughness increases up to 20.4 ± 3.0. AFM images revealed that the morphology of the blend is highly modified after 192 h of irradiation (Fig. 10b). It can be observed in the phase picture strong variations of contrast between the different areas, which indicates a phase separation at the surface. One can clearly observe, on the height and phase images after irradiation (Fig. 10b and c), two different phases with domains about 0.2–0.3 µm in diameter dispersed in a continuous matrix. This can be related to the DSC results, which showed two glass transition temperatures after ageing ascribed to a phase demixing phenomenon. The presence of PLA stereocomplexes has then a strong influence on the morphology of the blend during photochemical ageing. Such a phenomenon with phase separation in blends upon ageing has been reported by Hu et al. [45] in the case of PLA/PEG blends after thermal ageing.

In order to better characterize the morphology of the stereocomplex blend upon ageing, the surface of the samples were imaged using AFM peak-force QNM mode. Fig. 11 shows AFM height and modulus images (DMT model) of 60/40 blend (Figs. 11a) and 30/30/40 blend (Fig. 11b) after 192 h of irradiation.

From the modulus images, one can observe that the modulus of the 60/40 blend is mostly homogeneous after irradiation. On the contrary,

the AFM/DMT modulus image of the 30/30/40 blend after ageing shows separated domains of distinct modulus. In the black square represented in Fig. 11b, one can see that two features with the same average height present distinct modulus. We can particularly notice the presence of a lighter zone corresponding to a strong variation of mechanical properties.

This modification that does not involve any variation of the height of the sample highlights the presence of another phase. These domains have a diameter around 0.2–0.3 μm as already observed on Fig. 11b and c that show height and phase images. This confirms that the presence of PLA stereocomplexes in the 30/30/40 blend is responsible for a phase demixing phenomenon in photooxidative conditions, which was not observed in the case of the 60/40 PLA/PMMA blend.

The miscibility of PLLA/PMMA blends has already been deeply studied by C. Samuel et al. [14]. They showed that the control over the morphology of the blend depends on the thermal treatment, the processing conditions and molecular parameters of PLLA and PMMA. The use of high-molecular PLLA and PMMA was reported to promote the highest achievable properties upon melt-blending. The modifications at the molecular scale of PLA and PMMA during photodegradation change the polarity of the materials and the molecular parameters of the polymers. Therefore, this could explain the phase separation observed in the 30/30/40 blend.

As miscibility and stereocomplexation are key factors to designing shape memory performances materials, photostabilisation of the ternary stereocomplex blends is needed for successful applications of these materials in environments where light and air are involved.

4. Conclusion

This study on the photooxidation of PLA/PMMA blends showed that UV-light irradiation leads to strong modifications of the properties of these materials at every scale, molecular, macromolecular and morphology. The presence of stereocomplexes of PLA in the blends has a significant influence on the behavior of the blend during photochemical ageing.

Photooxidation of PLA and PMMA leads to the formation of carbonyl and hydroxyl products, detected by infrared analysis, which implies chain scissions and provokes a decrease of molecular weight evidenced by SEC measurements. The presence of PDLA and PMMA has no influence on the photooxidation rate of PLLA. Moreover, no prodegradant effect of the stereocomplexes on the photooxidation of the blends is observed.

However, the presence of PDLA has a strong influence on the thermal properties of the blend during photoageing. Indeed, the appearance of two glass transitions in 30/30/40 blend during ageing suggests that a phase separation occurs in this blend through photochemical ageing. This behavior was not noticed for 60/40 blend, which does not contain PLA stereocomplexes. The characterization by AFM of the morphology of the blends after ageing confirms this result. Two different phases with domains dispersed in a continuous matrix are observed for 30/30/40 aged sample, whereas 60/40 aged sample remains homogeneous after photooxidation.

This study clearly shows that UV-light with atmospheric oxygen significantly affects the properties of PLA/PMMA blends, and this is even more crucial in the presence of PLA stereocomplexes as the morphology is deeply modified, involving a phase separation phenomenon that can cancel the peculiar properties of the stereocomplex blend.

Acknowledgment

The authors wish to thank David Bourgogne for AFM peak-force images.

References

[1] R. Drumright, P. Gruber, D. Henton, Polylactic acid technology, Adv. Mater. 12 (2000) 1841–1846.
[2] R. Auras, B. Harte, S. Selke, An overview of polylactides as packaging materials, Macromol. Biosci. 4 (2004) 835–864.
[3] M. Murariu, A. Da Silva Ferreira, Ph Degée, M. Alexandre, Ph Dubois, Polylactide compositions. Part 1: effect of filler content and size on mechanical properties of PLA/calcium sulfate composites, Polymer 48 (9) (2007) 2613–2618.
[4] M. Pluta, M. Murariu, A. Da Silva Ferreira, M. Alexandre, A. Galeski, Ph Dubois, Polylactide compositions. II. Correlation between morphology and main properties of PLA/calcium sulfate composites, J. Polymer Sci. Part B Polymer Phys. 45 (19) (2007) 2770–2780.
[5] K. Molnár, J. Móczó, M. Murariu, Ph Dubois, B. Pukánszky, Factors affecting the properties of PLA/CaSO4 composites: homogeneity and interactions, Express Polym. Lett. 3 (1) (2009) 49–61.
[6] G. Gorrasi, V. Vittoria, M. Murariu, A. Da Silva Ferreira, M. Alexandre, Ph Dubois, Effect of filler content and size on transport properties of water vapour in PLA/calcium sulfate composites, Biomacromolecules 9 (3) (2008) 984–990.
[7] M. Murariu, A. Da Silva Ferreira, M. Pluta, L. Bonnaud, M. Alexandre, Ph Dubois, Polylactide (PLA)-$CaSO_4$ composites toughened with low molecular weight and polymeric ester-like plasticizers and related performances, Eur. Polym. J. 44 (11) (2008) 3842–3852.
[8] M. Murariu, L. Bonnaud, P. Yoann, G. Fontaine, S. Bourbigot, Ph Dubois, New trends in polylactic acid (PLA)-based materials: “Green” PLA-calcium sulfate (nano) composites tailored with flame retardant properties, Polym. Degrad. Stabil. 95 (3) (2010) 374–381.
[9] Dubois Ph, M. Murariu, M. Alexandre, Ph Degée, S. Bourbigot, R. Delobel, G. Fontaine, E. Devaux, Polylactide-based Compositions, (2008) WO patent 095874 Al.
[10] M. Murariu, A. Da Silva Ferreira, E. Duquesne, L. Bonnaud, Ph Dubois, Polylactide (PLA) and highly filled PLA-calcium sulphate composites with improved impact properties, Macromol. Symp. 272 (1) (2008) 1–12.
[11] A.J. Ryan, Polymer science: designer polymer blends, Nat. Mater. 1 (2002) 8–10.
[12] L.M. Robeson, Applications of polymer blends: emphasis on recent advances, Polym. Eng. Sci. 24 (8) (1984) 587–597.
[13] L.A. Utracki, History of commercial polymer alloys and blends (from a perspective of the patent literature), Polym. Eng. Sci. 35 (1) (1995) 2–17.
[14] C. Samuel, J.M. Raquez, Ph Dubois, PLLA/PMMA blends: a shear-induced miscibility with tunable morphologies and properties? Polymer 54 (2013) 3931–3939.
[15] D. Cossement, R. Gouttebaron, V. Cornet, P. Viville, M. Hecq, R. Lazzaroni, PLA-PMMA blends: a study by XPS and ToF-SIMS, Appl. Surf. Sci. 252 (2006) 6636–6639.
[16] X. Hao, J. Kaschta, X. Liu, Y. Pan, D.W. Schubert, Entanglement network formed in miscible PLA/PMMA blends and its role in rheological and thermo-mechanical properties of the blends, Polymer 80 (2015) 38.
[17] X. Hao, J. Kaschta, Y. Pan, X. Liu, D.W. Schubert, Intermolecular cooperativity and entanglement network in a miscible PLA/PMMA blend in the presence of nanosilica, Polymer 82 (2016) 57–65.
[18] C. Samuel, J.M. Raquez, Dubois Ph, Biobased poly(lactides)/poly(methyl methacrylate) blends: a perfect association for durable and smart applications? AIP Conference Proceedings, 2015, p. 1664.
[19] C. Samuel, S. Barrau, J.M. Lefebvre, J.M. Raquez, Ph Dubois, Designing multiple-shape memory polymers with miscible polymer blends : evidence and origins of a triple-shape memory effect for miscible PLLA/PMMA blends, Macromolecules 47 (2014) 6791–6803.
[20] T.P. Lodge, T.C.B. McLeish, Self-concentrations and effective glass transition temperatures in polymer blends, Macromolecules 33 (2000) 5278–5284.
[21] Y. Miwa, K. Usami, K. Yamamoto, M. Sakaguchi, M. Sakai, S. Shimada, Direct detection of effective glass transitions in miscible polymer blends by temperature-modulated differential scanning calorimetry, Macromolecules 38 (2005) 2355–2361.
[22] C. Samuel, J. Cayuela, I. Barakat, A. Müller, J.M. Raquez, Ph Dubois, Stereocomplexation of polylactide enhanced by poly(methylmethacrylate): improved processability and thermomechanical properties of stereocomplexable polylactide-based materials, ACS Appl. Mater. Interfaces 5 (2013) 11797–11807.
[23] L.A. Utracki, Polymer Blends Handbook, Springer, Berlin, 2002.
[24] Y. Ikada, K. Jamshidi, H. Tsuji, S. Hyon, Stereocomplex formation between enantiomeric poly(lactides), Macromolecules 20 (1987) 904–906.
[25] H. Tsuji, Poly(lactide) stereocomplexes: formation, structure, properties, Degradation, and Applications. Macromolecular Bioscience 5 (2005) 569–597.
[26] S. Bocchini, S. Therias, J.L. Gardette, G. Camino, Influence of nano-dispersed boehmite on polypropylene photooxidation, Polym. Degrad. Stabil. 92 (10) (2007) 1847–1856.
[27] M. Gardette, S. Therias, J.L. Gardette, M. Murariu, Ph Dubois, Photooxidation of polylactide/calcium sulphate composites, Polym. Degrad. Stabil. 96 (2011) 616–623.
[28] R. Drumright, P. Gruber, D. Henton, Polylactic acid technology, Adv. Mater. 12 (23) (2000) 1841–1846.
[29] H. Tsuji, T. Saeki, T. Tsukegi, H. Daimon, K. Fujie, Comparative study on hydrolytic degradation and monomer recovery of poly(L-lactic acid) in the solid and in the melt, Polym. Degrad. Stabil. 93 (10) (2008) 1956–1963.
[30] Y. Tokiwa, B.P. Calabia, Biodegradability and biodegradation of poly(lactide), Appl. Microbiol. Biotechnol. 72 (2) (2006) 244–251.
[31] G. Kale, A. Rafael, S.P. Singh, R. Narayan, Biodegradability of polylactide bottles in

real and simulated composting conditions, Polym. Test. 26 (8) (2007) 1049–1061.
[32] R. Auras, B. Harte, S. Selke, An overview of polylactides as packaging materials, Macromol. Biosci. 4 (9) (2004) 835–864.
[33] H. Tsuji, In vitro hydrolysis of blends from enantiomeric poly(lactide)s. 1. Well-stereocomplexed blend and non-blended films, Polymer 41 (10) (2000) 3621–3630.
[34] H. Tsuji, Y. Echizen, Y. Nishimura, Photodegradation of biodegradable polyesters: a comprehensive study on poly(L-lactide) and poly(3-caprolactone), Polym. Degrad. Stabil. 91 (5) (2006) 1128–1137.
[35] L. Zaidi, M. Kaci, S. Bruzaud, A. Bourmaud, Y. Grohens, Effect of natural weather on the structure and properties of polylactide/Cloisite 30B nanocomposites, Polym. Degrad. Stabil. 95 (2010) 1751–1758.
[36] H. Tsuji, H. Sugiyama, Y. Sato, Photodegradation of Poly(lactic acid) stereocomplex by UV-irradiation, J. Polymer Environ. 20 (2012) 706–712.
[37] N. Siampiringue, J.P. Leca, J. Lemaire, Mécanismes de photo-oxydation du poly (methacrylate de methyle), Eur. Polym. J. 27 (7) (1991) 633–641.
[38] S. Jacobsen, H.G. Fritz, Ph Degée, Ph Dubois, D. Jérôme, Single-step reactive extrusion of PLLA in a corotating twin-screw extruder promoted by 2-ethylhexanoic acid tin(II) salt and triphenylphosphine, Polymer 41 (9) (2000) 3395–3403.
[39] J. Lemaire, J.L. Gardette, Aging of polymers. Principles of the study of photoaging, Revue Generale du Caoutchouc et des Plastiques 613 (1981) 87–92.
[40] J. Lemaire, J. Lacoste, N. Siampiringue, Predicting the weatherability of polymerics materials within the mechanistic approach based on artificial accelerated and ultraaccelerated photoageing equipements, Materia Raifu Gakkaishi, J. Mater. Life Soc. 22 (2010) 50–57.
[41] E.W. Fisher, H.J. Sterzel, G. Wegner, Investigation of the structure of solution grown crystals of lactide copolymers by means of chemical reactions, Colloid Polym. Sci. 251 (1973) 980–990.
[42] H. Tsuji, T. Tsuruno, Accelerated hydrolytic degradation of Poly(l-lactide)/Poly(d-lactide) stereocomplex up to late stage, Polym. Degrad. Stabil. 95 (4) (2010) 477–484.
[43] S. Therias, J.F. Larché, P.O. Bussiere, J.L. Gardette, M. Murariu, Ph Dubois, Photochemical behavior of polylactide/ZnO nanocomposite films, Biomacromolecules 13 (2012) 3283–3291.
[44] J. Gaume, A. Rivaton, S. Therias, J.L. Gardette, Influence of nanoclays on the photochemical behaviour of poly(vinyl alcohol), Polym. Degrad. Stabil. 97 (2012) 488–495.
[45] Y. Hu, M. Rogunova, V. Topolkaraev, A. Hiltner, E. Baer, Aging of poly(lactide)/poly(ethylene glycol) blends. Part 1. Poly(lactide) with low stereoregularity, Polymer 44 (2003) 5701–5710.